Contemporary (2016–2020) land cover across West Antarctica and the McMurdo Dry Valleys

Christopher D. Stringer[1], Jonathan L. Carrivick[1], Duncan J. Quincey[1] , Daniel Nývlt[2]

[1]School of Geography and water@leeds, University of Leeds, Woodhouse Lane, Leeds, West Yorkshire LS2 9JT, UK
[2]Polar-Geo-Lab, Department of Geography, Faculty of Science, Masaryk University, Kotlářská 2, CZ-611 37 Brno, Czech Republic

Correspondence to: Christopher D. Stringer (gycds@leeds.ac.uk)

Abstract. Continental-scale land cover information is essential to furthering our understanding of the terrestrial environment, atmosphere and climate change. Several global land cover products have been released in recent years but they typically do not include Antarctica. The lack of land cover data in Antarctica is concerning because mountain glaciers and icecaps there have been losing mass at a rate well above the global average, leading to expansion of proglacial regions. Proglacial regions comprise transient land cover types with high rates of geomorphological activity that delivers sediment into the Southern Ocean and supports its rich biodiversity. With Antarctic mountain glaciers and icecaps projected to lose more mass in the coming decades, and active layer soils expected to increase in thickness, it is timely to establish a baseline land cover dataset for Antarctica with which future classifications can be compared. Here, we use Landsat-8 Operational Land Imager (OLI) images to classify six proglacial regions of Antarctica at 30 m resolution, with an overall accuracy of 77.0 % for proglacial land classes. We conducted this classification using an unsupervised K-means clustering approach, which circumvented the need for training data and was highly effective at picking up key land classes, such as vegetation, water, and different sedimentary surfaces. We have highlighted the spatial pattern in land cover and emphasise a need for more and higher quality field data. The land cover maps produced from this paper are available at: Stringer, C. (2022). Contemporary (2016 - 2020) land cover classification across West Antarctica and the McMurdo Dry Valleys (Version 1.0) [Data set]. NERC EDS UK Polar Data Centre. https://doi.org/10.5285/5A5EE38C-E296-48A2-85D2-E29DB66E5E24

1. Introduction

Continental-scale land cover information is essential to furthering our understanding of terrestrial environments, ecological niches and the atmosphere, especially across sensitive regions of Earth (Ban et al., 2015; Chen et al., 2019; Gong et al., 2020; Raup et al., 2007). Additionally, land cover maps are a critical resource required to support research of climate change: particularly those that include information on vegetation coverage (Bojinski et al., 2014). Different types of land cover can change or respond to climatic forcing in different ways, depending on their physical and chemical properties (GCOS, 2010).

Owing to the frequent return period and extensive areas covered by satellite images, land cover maps are increasingly being produced using remote-sensing techniques (Brown et al., 2022; Friedl et al., 2010; Loveland et al., 2000; Tateishi et al., 2014). Several global land cover products have been released in recent years (e.g. Brown et al., 2022) but they typically do not include Antarctica. Land cover maps are particularly important for Antarctica, owing to its dynamic landscape and rapid environmental

35 change (Davies et al., 2013). Unlike most other regions on Earth, human activities are not the major control on land cover type in Antarctica, and the footprint of anthropogenic activities is limited to relatively small areas (Tejedo et al., 2016, 2022). Until the start of the 21st century, the Antarctic Peninsula (AP) was one of the most rapidly warming places on Earth with a temperature rise of 1.5 °C observed since the 1950s (Bentley et al., 2009; Cannone, 2020; Carrivick et al., 2012; Guglielmin, 2020; Kavan et al., 2017; Mulvaney et al., 2012; Oliva et al., 2016; Vaughan et al., 2003). Following a hiatus in warming at

40 the start of the 21st century, there is evidence that this trend has resumed (Carrasco et al., 2021) and glaciers have continued to respond to the temperature increases of the 20th century and subsequent warming since 2015 (Engel et al., 2022; Oliva et al., 2017). Consequently, glacier mass loss has occurred at an enhanced rate, particularly around smaller ice masses on the AP and on sub-Antarctic islands (Abram et al., 2013; Engel et al., 2022; Oliva et al., 2016, 2017; Rosa et al., 2020). This ice mass loss has resulted in the enlargement of some of Antarctica's proglacial regions, and they will continue to expand as both land and

45 marine-terminating glaciers continue to retreat with a warming climate (Nedbalová et al., 2013; Roman et al., 2019). It is, therefore, essential to have a baseline with which to compare past and future changes in these environments.

The majority (99.8 %) of Antarctica is covered by ice, with the remaining 0.2 % characterised as nunataks (i.e. mountain peaks that penetrate the ice sheet) or as proglacial regions (Burton-Johnson et al., 2016). Proglacial regions are predominantly shaped

50 by the interplay of meltwater from glaciers, which erodes, transports and deposits sediment, and hillslope activity, which largely acts to supply new sediment into the system during mass transport events. In a warming climate both result in greater sediment discharge (Klaar et al., 2015; Ballantyne, 2008; Staines et al., 2015; Carrivick and Heckmann, 2017; Carrivick and Tweed, 2021). In polar regions, where permafrost can be extensive, the active layer is an additional and important water and sediment source on days where ground temperatures exceed 0 °C (Costa et al., 2018; Humlum et al., 2003; Kavan et al., 2017;

55 Łepkowska and Stachnik, 2018). Understanding the make-up of Antarctica's proglacial regions is important because they are a source of water, sediment and solutes. The quantity and spatio-temporal pattern of sediment discharged from Antarctica has profound effects on the ecosystem of the Southern Ocean and polar lakes, with particular impacts seen in benthic communities (Friedlander et al., 2020). The majority of sediment enters these ecosystems via rivers (Overeem et al., 2017) and suspended sediments impact the feeding behaviour of marine and lacustrine organisms. Large quantities of sediment increase the turbidity

60 of the water; this prevents photosynthesis and can lead to organisms ingesting sediment and suffering mechanical damage (Cloern, 1987; García-Rodríguez et al., 2021; Laspoumaderes et al., 2013; Maat et al., 2019; Sommaruga, 2015). The quantity of sediment entering polar waters in the summer months is also thought to play a role in the size of phytoplankton blooms (Arrigo et al., 2017; García-Rodríguez et al., 2021; Leeuwe et al., 2020; Righetti et al., 2019). These factors may alter the quantity of carbon that is sequestered from the atmosphere by these organisms (Brussaard et al., 2008; Maat et al., 2019).

65   Given the clear importance of land cover, and more specifically sediment dynamics, to the functioning of Antarctic ecosystems, the aims of this paper are: **i)** produce a map of land cover across selected proglacial areas of West Antarctica and the Dry Valleys, and; **ii)** quantify the overall accuracy of our data and how that accuracy varies spatially.

1.1 Study Sites

There is a notable dearth of literature that seeks to characterise proglacial regions, particularly in Antarctica. Some research
70   has been conducted on individual rivers and catchments, notably on the Onyx River (Chinn and Mason, 2016), James Ross Island's Ulu Peninsula (e.g. Davies et al., 2013; Jennings et al., 2021; Kavan, 2021; Kavan et al., 2020, 2017; Nedbalová et al., 2013) and on other sub-Antarctic islands, such as the South Shetland Islands (Mink et al., 2014; Oliva et al., 2016). However, these studies have taken varying approaches to characterising landscape compositions, and there is little in way of a continental scale dataset that characterises the land cover of these proglacial regions in a consistent way. Therefore, we have
75   chosen six sites for analysis in this study that are characterised by their large proglacial area (Fig. 1). Namely, these sites are: **i)** the McMurdo Dry Valleys; **ii)** Alexander Island and west Palmer Land (referred to hereafter as "Alexander Island"); **iii)** Deception Island; **iv)** southern Livingston Island and Snow Island (referred to hereafter as Byers Peninsula); **v)** James Ross Archipelago, and; **vi)** South Georgia.

1.1.1 Climate

80   All of the six study sites have polar climates and comprise both maritime and continental settings. They are positioned along a latitudinal gradient and so permit an analysis of land cover variability with latitude. The most northern site, South Georgia, is characterised by its high relief and has a mean annual air temperature (MAAT) of 2.5 °C, as well as receiving over 2000 mm of precipitation per year (Bannister and King, 2015; Strother et al., 2015). Over half of South Georgia is glacierised (Bannister and King, 2015). The South Shetland Islands are characterised by a polar maritime climate, with air temperatures
85   regularly exceeding 0 °C in summer. The humid environment, due to its maritime location, ice-free seas and regular cyclonic activity, results in liquid precipitation falling regularly in the summer months (Bañón et al., 2013). The James Ross Archipelago, to the north-east of the Antarctic Peninsula, has a MAAT of -7 °C and has a semi-arid polar continental climate (Hrbáček and Uxa, 2020; Martin and Peel, 1978). The two more southerly sites; Alexander Island and The McMurdo Dry Valleys, are distinctly colder and drier than the more northern sites, with continental climates (Harangozo et al., 1997).
90   Alexander Island, specifically Fossil Bluff, has a MAAT of -9 °C and receives approximately 900 mm of precipitation each year (Davies et al., 2017; Harangozo et al., 1997). The McMurdo Dry Valleys are hyper-arid due to katabatic winds and have a MAAT of -17 °C to -20 °C (Doran et al., 1994; Marchant and Head, 2007).

2. Methods

2.1. Site Selection

95 Our site selection was primarily informed by the British Antarctic Survey's (BAS) rock outcrop dataset (Gerrish et al., 2020), allowing us to focus primarily on the non-glacierised landscape. Nunataks in the interior of the ice sheets were excluded because they were too small to classify at 30 m resolution, and we could assume their classification to be bedrock. Since they are disconnected from the coastline, they can be assumed largely unimportant as sediment sources to the Southern Ocean. Fossil Bluff and other coastal regions in Alexander Island and Palmer Land were included and are interesting for their

100 proximity to George VI Sound. These regions will potentially become important sediment sources in the near future, as exceptional melting in this region has increased the risk of the Georgie VI ice shelf collapsing (Banwell et al., 2021). We further narrowed the site choices to consider only those regions with cloud-free Landsat-8 Operational Land Imager (OLI) images.

2.2. Land cover classifications

105 In the last decade, medium-resolution satellite data from the Landsat and Sentinel programmes have become open source and increasingly easy to access. In tandem with improved computational power, such as that provided by cloud-based platforms like Google Earth Engine, it is now possible to produce land cover maps at a medium spatial resolution (10 m to 30 m) using openly available data. The Landsat-8 satellite also has the benefit of being part of a continuation programme that has five decades of images, making inter-decadal comparison possible with images taken as long ago as 1972.

110 ### 2.2.1. Image selection and pre-processing

We classified Landsat-8 OLI images acquired between 2016 and 2020 (see Appendix B for details) in Google Earth Engine (GEE) and ESRI ArcGIS Pro 2.6.0, primarily using K-means clustering. We chose Landsat imagery, rather than other satellite image sources (such as Sentinel-2), because of its extensive archive dating back to 1972, making any future comparisons with our baseline dataset as robust and as seamless as possible. Suitable images had low cloud cover (less than 20 % over land) and

115 limited snow cover, meaning that for some sites we were limited to a single image for analysis. Where more than one image was available, we mosaicked them taking the most suitable pixels from each, thus minimising the snow and cloud cover across the unified scene.

To ensure consistency with older Landsat images, we selected six bands representing the visible and infrared wavelengths (ranging from 0.45 to 2.29 μm) from the images for classification. We added three further bands to the image in the form of

120 normalised difference snow index (NDSI, Eq. 1), normalised difference vegetation index (NDVI, Eq. 2), and normalised difference water index (NDWI, Eq. 3). These aided the classifier in the identification of key land cover types (ice, vegetation, and water, respectively).

$$NDSI = \frac{green - swir1}{green + swir1} \qquad (1)$$

$$NDVI = \frac{nir - red}{nir + red} \qquad (2)$$

125

$$NDWI = \frac{green - nir}{green + nir} \qquad (3)$$

Where:

green = band 3 of Landsat 8 OLI, wavelength (λ) = 0.53–0.59 μm

swir1 = shortwave infrared 1, band 6, λ = 1.57–1.65 μm

red = band 4, λ = 0.64–0.67 μm

130   nir = near infrared, band 5, λ = 0.85–0.88 μm

We topographically corrected the images using the REMA DSM (Reference Elevation Model of Antarctica mosaic Digital Surface Model) (Howat et al., 2019) at 30m resolution (equivalent to the resolution of Landsat-8 OLI multispectral bands). South Georgia, which isn't covered by REMA, was corrected using the SRTM DEM (Shuttle Radar Topography Mission

135   Digital Elevation Model), also at 30m resolution (Farr et al., 2007). Subsequently, we conducted a principal component analysis of the images in GEE and the first three components, containing 99.6 % (± 0.3 %) of the data, were selected (Chasmer et al., 2020; Frohn et al., 2009).

2.2.2. Classification

We used a hierarchical approach to image classification. A first order land classification of "land", "ice", and "water" informed

140   the subdivision of each of these classes in a second, more detailed, analysis of the dominant land cover types. To produce these broad land classes, we used a K-means clustering algorithm in GEE to split each image into 75 (K value = 75) discrete clusters. This K value was determined through trial and error, and it represents a compromise that minimised both the chance of misclassification and computation time. The clusters are determined using the spectral information of each image, based on 500,000 randomly selected sampling points. We assigned each of these sections a first order class in ArcGIS by visually

145   inspecting the image they were derived from. In some cases, we could not easily assign a cluster a first order class. This was usually because a cluster had conflated shadow with dark seawater. To address this, we split these clusters using a slope threshold of 3°, with pixels <3° being assigned as water. Where this process resulted in obvious misclassification we used a random forest classifier to differentiate between water, land and ice. Some pixels were covered entirely by very dark shadows or clouds and, therefore, we could not classify them; these were assigned "No data".

150

We used this first order land classification to subset each image in GEE accordingly, and then to cluster these resulting images into 40 discrete groups (K = 40). Using the limited catalogue of published maps and literature available for these areas (see

Table 1); we interpreted these clusters to manually assign each of them a final land classification. Our first-order land class was subset into five classes "Bedrock", "Coarse/wet sediment", "Fine & dry sediment", "Vegetation", and "Land (non-differentiated)". The water class subset into "Water" and "Turbid water", while the ice class subset into "Ice" and "Wet ice". In cases where clouds partially obscured land, we assigned pixels to the more general class of "Land (non-differentiated)". Therefore, we produced ten land classes that describe eight distinct surface types, plus partially obscured land (Land (non-differentiated)), and surfaces totally obscured by clouds or shadows (No data). The largest of these examples are on South Georgia and James Ross Island. To the northwest of South Georgia (Cape Alexandra and Bird Island), we classified a large area of land as "no data", since it was entirely obscured by thick clouds in images. Similarly, we classified the southeast of James Ross Island (the largest island in the James Ross Archipelago) as "land (undifferentiated)". This region was covered by thin clouds in the imagery, which allowed us to differentiate land from ice and water, but it meant that we could not assign the land a second-order class with any confidence.

Table 1: Resources used to interpret clusters and assign them to a land class

Location	Resources
James Ross Island	Geomorphology map, Jennings et al. (2021)
	Geomorphology map, Davies et al. (2013)
	Geological map (British Antarctic Survey), Smellie et al. (2013)
	Geological map (Czech Geological Survey) (Mlčoch et al., 2020)
	Vegetation map (Barták et al., 2015)
Dry Valleys	Interactive geological map (SCAR) (Cox *et al.,* 2019)
Alexander Island	Geological map of Alexander Island (British Antarctic Survey, 1981)
Deception Island	Geology and geomorphology Map (BAS) (Smellie *et al.,* 2002)
	ASPA 140: Parts of Deception Island, South Shetland Islands (Secretariat of the Antarctic Treaty, 2022)

| **Livingston Island** | Geomorphological map of Byers Peninsula, Livingston Island (Lopez-Martinez *et al.*, 1996) |
| **South Georgia** | Geomorphology of the Stromness Bay-Cumberland Bay area, South Georgia (Clapperton, 1971) |

2.3. Accuracy Assessment

170   Having used the limited pre-existing land cover data to inform our interpretation of the K-means clusters, we had to depend on finer-resolution imagery as the primary independent validation source. Although we could not find alternative land cover data, we still used the methods of best practice described by Olofsson et al. (2013, 2014) to ensure our accuracy assessment was robust. Therefore, we generated 3000 random points, stratified by the area of each land class, and visually compared them to 10 m resolution Sentinel-2 MultiSpectral Instrument (MSI) images. Given the dominance of the ice class in our classification, this meant most of the stratified sample points landed on ice. We conducted a second level of accuracy

175   assessment with 1000 points on just the proglacial classes to ensure their accuracy was adequately calculated.

The classes of turbid water and wet ice were particularly problematic because they typically comprised episodic sediment plumes and snow/ice melt. Therefore, we combined these classes with water and ice respectively for the purposes of accuracy assessment. We produced a 10 km resolution grid to display the spatial variability in the accuracy of this classification (as a

180   proxy for confidence), with each cell colour coded according to the percentage of accurate assessment points within it.

2.4. Code availability

The codes used in these methods are available at:

Christopher D Stringer. (2022). Contemporary (2016–2020) land cover across West Antarctica and the McMurdo Dry Valleys [Code] (Version 1). Zenodo. https://doi.org/10.5281/zenodo.6720051

185   **3. Results and Discussion**

3.1. Land cover classifications

3.1.1. The land classes

The largest land class at our sites is ice; the large ice sheets and glaciers at all sites have been successfully mapped, making this dataset a particularly useful resource to look at the small, land-terminating glaciers in Antarctica (Fig. 3). Of the proglacial

190   land classes, the two sedimentary classes (coarse/wet sediment and fine and dry sediment) are the dominant land classes (Fig.

3). During the clustering process, we created two different sedimentary classes because we found that pixels containing wet sediments (such as rivers) or blocky superficial sediments, such as scree, clustered distinctly from those pixels that contain sediments smaller than cobbles in size and fissile sedimentary rocks. This grain size threshold was derived from information on geomorphological maps for the region (Jennings et al., 2021), and observations made on James Ross Island during the 2022 field season. We emphasise that the first of these two classes describes pixels that contain sediment that may be coarse, wet, or both. The second of these classes describes surfaces with fine sediments with minimal water content.

Of these sedimentary classes, coarse and wet sediment is the predominant land class at four of the six sites, particularly on South Georgia and Byers Peninsula, where it represents the majority (57 % and 56 % respectively) of the proglacial land cover (Fig. 4). This land class includes the drainage networks of Antarctica, and this is particularly notable on James Ross Island (Fig. 2) and in the McMurdo Dry Valleys, where it accurately depicts major rivers; the Bohemian Stream, Abernethy River and Onyx River are particularly clear. The fine and dry sediment class is dependent upon the quantity of coarse/wet sediment; where there is a greater proportion of coarse/wet sediment there is less fine and dry sediment and vice versa. For example, on South Georgia, the 57 % coverage of coarse sediment is in comparison to a 33 % coverage of fine and dry sediment. On Deception Island, where fine and dry sediments are the dominant land class (53 %), there is only 26 % coverage of coarse/wet sediment (Fig. 4). At all of the sites, between 70 % and 80 % of the proglacial surface is covered by sediment.

The bedrock class, which primarily describes igneous and metamorphic rock surfaces, is most abundant on Deception Island, covering 14 % of its proglacial areas (Fig. 4). In the Dry Valleys, bedrock covers 13 % of the area and the performance of the classification is particularly notable for its ability to pick out an exposed basement sill (Petford and Mirhadizadeh, 2017) in Wright Valley. In other studies (e.g. Jennings et al., 2021), bedrock classes are often over-represented (Fig. 2), because the aim of the study is to map geomorphology or geology, rather than surface characteristics such as physical weathering and *in situ* production of block fields. Moreover, field observations show that boulders and other glacigenic sediments overlie many of the large igneous extrusions. Therefore, our classification gives a better sense of the surface extent of exposed solid bedrock.

The classes relating to water (water, turbid water, wet ice) are of varying quantities across all of the sites. The wet-ice class proved to be a little ambiguous to interpret from clusters, and represents saturated firn and 'slush' ice (i.e. partially melted ice or partially frozen water). Wet ice is most abundant on Alexander Island, with 17 % coverage (Fig. 4), and highlights the record-high surface melt observed around the King George VI Ice Shelf in late 2019 (Banwell et al., 2021). This large amount of wet ice is comparable to James Ross Archipelago (15 %), where a large proportion of wet ice is accounted for by a melt event that resulted in a large area of saturated firn on Snow Hill Island (Fig. 5). This transient nature of wet ice is also seen with the turbid water class, which can pick out sediment plumes (Fig. 5).

Our land classification also provides the first large-scale map of vegetation in Antarctica. Notably, this includes the large fields

225 of vegetation on South Georgia, which we have calculated to cover 8 % of its proglacial surface and are clearly identifiable in satellite images (Fig. 4). We have also identified several sites of vegetation on the South Shetland Islands; especially those on Deception Island (total 1 % surface coverage, Fig. 4) within ASPA 140 (sub site B) on Deception Island (Secretariat of the Antarctic Treaty, 2022). In some cases, we have even been able to identify very small areas of vegetation such as those that we identified on James Ross Island that were verified in the field (Fig. 2).

230 **3.1.2. Spatial variations**

We observe a spatial variation in land cover between the sites (Fig. 4). There is typically more coarse/wet sediment at sites further away from the pole; this is offset by a general decrease in fine and dry sediments. However, the Dry Valleys are an exception to this, with 44 % of the land covered by coarse or wet sediments. The second most southern site, Alexander Island, has 0 % of its proglacial surface covered by coarse/wet sediment, compared with 57 % on South Georgia.

235

Unlike other land classes, the proportion of the water and wet ice classes appears to be more evenly spread across the sites. There is a slight apparent latitudinal trend in these data, with more water at the sites further to the north, and a variability between the east and west (i.e. when comparing the South Shetland Islands with James Ross Archipelago, Fig. 4). South Georgia and Byers' Peninsula have the largest amount of liquid water present (when joining the water and turbid water classes

240 together), around 3 %. James Ross Archipelago has significantly less (1 %) and Alexander Island has 1% of its surfaces classified as water, owing to a large amount of supraglacial water at the time of image acquisition. We classified some of this melt as water, rather than wet ice, as it was unambiguously liquid when we inspected and interpreted the clusters. The bedrock class does not show a clear latitudinal trend, and is most abundant in Deception Island (14 %) and the McMurdo Dry Valleys (13 %).

245

The most northern site of South Georgia had significantly more vegetation than any other site (7 % of the proglacial regions are covered by vegetation, Fig. 4), while the McMurdo Dry Valleys and Alexander Island have no detectable vegetation coverage. James Ross Island has very little vegetation cover (< 1 %), while the South Shetland Islands show 2 % coverage on Byer's Peninsula and 1 % on Deception Island.

250 **3.1.3. Potential drivers of variability**

The trends in sedimentary classes are consistent with the expectation that greater runoff should occur in polar regions with higher temperatures (Syvitski, 2002). Increased runoff would result in a greater proportion of the surface being covered by the coarse/wet land class. However, the Dry Valleys are an exception to this, with 44 % of the land covered by coarse or wet sediments (Fig. 4). This is likely due to the high relief of the region, allowing for greater mass movement and scree formation

255 (Doran et al., 2002; Kirkby and Statham, 1975), and consistent solar radiation during the austral summer facilitating glacier

melt and the formation of large rivers such as the Onyx River (Conovitz et al., 2013; Gooseff et al., 2011). We did not identify any coarse sediment on Alexander Island. The reasoning for this is two-fold: **i)** an apparent lack of major drainage networks, and; **ii)** the scree slopes in this region appear to be small and thin. When viewed from Sentinel-2 images, we could identify only small-size scree slopes and very few streams, consistent with observations made by Heywood et al. (1977), who noted

260 that many scree slopes were composed of fine sediments. Alexander Island, in particular, was difficult to classify due to a lack of supporting material to aid our cluster interpretations; the most recent geological map is from 1981 (British Antarctic Survey, 1981) and only limited geomorphological maps of the region exist (e.g. Salvatore, 2001). This site highlights the need to collect more high-quality ground data in Antarctica, in order to improve our wider understanding of proglacial environment in the southernmost continent. Even projects to map small areas of these remote regions would improve the performance of remote

265 techniques, such as those described in this study.

The trends in the wet ice, water and turbid water classes show more water at the sites further to the north, and a variability between the east and west, likely due to climatic conditions favouring liquid water on the South Shetland Islands and South Georgia. The disproportionately large amount of water and wet ice on Alexander Island and the James Ross Archipelago

270 relates to the high melt in these areas at the time of image acquisition, as previously discussed. The bedrock class is most abundant on Deception Island and McMurdo Dry Valleys, owing to ongoing volcanism on Deception Island (Rosado et al., 2019; Smellie et al., 2002) and extensive volcanic history of the McMurdo Dry Valleys (Petford and Mirhadizadeh, 2017; Smellie and Martin, 2021). This class is also associated with volcanic rocks on James Ross Island (Jennings et al., 2021; Mlčoch et al., 2020), Byers Peninsula (Gao et al., 2018) and metamorphic rocks outcrops on Alexander Island (British Antarctic

275 Survey, 1981).

We noted a latitudinal trend in the presence of vegetation, with the largest proportions of vegetation coverage observed on South Georgia and the South Shetland Islands, and no coverage on Alexander Island or the McMurdo Dry Valleys. This is consistent with observation made in Arctic regions, where regions closer to the poles have significantly less vegetation

280 coverage (Walker et al., 2018). Although no vegetation was detected in Alexander Island or the McMurdo Dry Valleys, small areas of vegetation have previously been described (Heywood et al., 1977; Pannewitz et al., 2003), though they are typically below the scale of our classification. Latitude is not the only indicator of vegetation coverage, though. The sparse vegetation coverage on James Ross Island, despite its relatively low latitude, is consistent with field observations and is logical given its semi-arid climate and high wind-speeds (Barták et al., 2015; Davies et al., 2013; Hrbáček and Uxa, 2020; Kňažková et al.,

285 2021; Martin and Peel, 1978; Nývlt et al., 2016). Deception Island has less vegetation than the neighbouring Byers' Peninsula, perhaps due to the impact of ongoing volcanic activity on the island and relatively recent eruptions resulting in unfavourable conditions (Collins, 1969; Smith, 1988, 2005).

3.2. Data accuracy

3.2.1. Overall accuracy

290 The overall accuracy of our land classification is 95.9 %. However, this overall value should be taken with caution, since a large proportion of our areas of analysis are covered by ice. This high accuracy represents the fact that our model is very effective at differentiating ice from land and water. The accuracy of each land class individually provides a more informative assessment of this model. We find that each proglacial land class has a relatively large standard error, owing to the small numbers of pixels that we checked (Table 2).

295

Table 2: Accuracy assessment of all land classes. NB: n<3000 as several points landed on cloud-covered parts of the reference images. % error refers to the size of the 95% confidence bounds, relative to the error adjusted area.

Class	Error adjusted area (km²)	95% confidence (km²)	% Area	% error	n
Water	99.1	45.5	0.2	45.9	9
Ice	44 001.5	219.6	92.2	0.5	2 595
Bedrock	231.3	174.2	0.5	75.3	27
Fine & dry sediment	2 131.5	195.9	4.5	9.2	134
Coarse/wet sediment	1 156.6	174.2	2.4	15.1	114
Vegetation	115.7	56.4	0.2	48.8	10

The overall accuracy of the proglacial component of the classification is 77.0%, with the greatest percentage uncertainty in the

300 smaller sized land classes (water and vegetation). While this overall accuracy is slightly lower than some products (e.g. Pazúr et al., 2022; Malinowski et al., 2020), it should be noted that we achieved this without extensive training data, making it more comparable with the more moderate accuracies achieved by Chen et al., 2015, for example. The sediment classes typically perform well, with relatively small percentage errors (Table 3). The accuracy matrices can be found in Appendix A.

305 Since we were unable to assess the accuracy of the turbid and wet ice classes, we have provided an example of a classification of each land class, to allow for qualitative assessment of its accuracy (Fig. 7).

Table 3: Accuracy assessment of proglacial classes. NB: n<1000 as several points landed on cloud-covered parts of the reference images. % error refers to the size of the 95% confidence bounds, relative to the error adjusted area.

Class	Error adjusted area (km²)	95% confidence (km²)	% Area	% error	n
Water	85.7	26.4	2.0	30.9	15
Bedrock	285.5	56.7	6.6	19.9	45
Fine & dry sediment	2 375.5	106.9	54.7	4.5	371
Coarse/wet sediment	1 444.7	108.8	33.3	7.5	257
Vegetation	148.5	40.1	3.4	27.0	34

310

3.2.2. Spatial confidence

We produced a map to represent the confidence of our dataset (Fig. 8), which is notable for its spatial homogeneity; no individual site appears to be more or less accurate than any other. The McMurdo Dry Valleys have the most "very low confidence" cells, but this is a function of it being the second largest site analysed, with the largest extent of proglacial land

315   cover. Since proglacial classes are less accurate than ice (Table 2 and Table 3), it is to be expected that the greatest amount of "very low confidence" cells would be present here. We also observed that many of these "very low confidence" cells contain only one or two assessment points. This means that just one inaccurate point may result in the cell being classified as "very low confidence", when in fact further analysis may reveal it performs better than is represented here.

We also note that the highest accuracy, i.e. the regions with the highest density of "very high confidence" cells, are within the

320   ice sheets at each site, which is consistent with the analysis (Table 2). This is particularly clear on South Georgia and Alexander Island. The regions with "no points" are primarily over the large ice sheets, particularly to the centre of James Ross Island, Alexander Island and the Dry Valleys. Because of the large extent of ice, many cells were not checked during the accuracy assessment because the random points algorithm in GEE did not assign a point to each cell. However, in reality, we are highly confident of cells within the centre of ice sheets: they are clearly ice when inspected and the 92.4% accuracy of the ice class

325   (Table 2) suggests they are very likely to be accurate.

3.3. Data availability

The data used to produce these results, alongside the sampling points for the accuracy assessment and the spatial map of confidence, are available as TIFs and shapefiles at:

Stringer, C. (2022). Contemporary (2016 - 2020) land cover classification across West Antarctica and the McMurdo Dry

330   Valleys (Version 1.0) [Data set]. NERC EDS UK Polar Data Centre. https://doi.org/10.5285/5A5EE38C-E296-48A2-85D2-E29DB66E5E24

4. Summary and conclusions

In this study, we have documented the first continental scale land cover map of largely non-glacierised areas of West Antarctica

335 and the McMurdo Dry Valleys and we have achieved this using an unsupervised K-means clustering approach in Google Earth Engine at 30 m resolution. Our chosen sites comprise the largest proglacial regions across Antarctica and we have produced these data to further research in a number of disciplines, particularly those projects in ecology, environmental sciences and atmospheric sciences. We present information on the extent of several land cover types, notably vegetation, water, and sedimentary surfaces. We have mapped 10 land classes at 30 m resolution that describe eight distinct surfaces at an accuracy

340 of 77.0 % for proglacial classes, and 92.2% for ice. We have also highlighted the spatial variability in land classes, notably in vegetation and coarse/wet sediment, which are typically more abundant in sites that are more northerly located. Our research has also highlighted the need for greater ground-verified data to improve the accuracy of future Antarctic land classifications.

Author contribution

CS produced the data, conducted the analysis and wrote the manuscript. JC, DQ, and DN supervised the project and contributed

345 to the writing.

Acknowledgements

The Czech Antarctic Research Programme (CARP) are thanked for their support of this project, particularly in accommodating CS at the Johann Gregor Mendel Research Station on James Ross Island during the austral summer of 2021/22. We also thank all of the staff at CARP for their logistical support. Michael Grimes and Elizabeth Mroz of the University of Leeds and Jan

350 Kavan of Masaryk University are thanked for their technical support. The British Antarctic Survey (BAS) and Stephen Jennings provided maps of Alexander Island and James Ross Island respectively that made this study possible. BAS also provided other resources, including maps and aerial imagery that was not directly used in this study, but was very much appreciated.

This work is supported by the Leeds-York-Hull Natural Environment Research Council (NERC) Doctoral Training Partnership

355 (DTP) Panorama under grant NE/S007458/1. The Ministry of Education, Youth and Sports of the Czech Republic project VAN 1/2022 and the Czech Antarctic Foundation funded fieldwork that contributed to part of this work.

Competing interests

The authors declare that they have no conflict of interest.

References

360   Abram, N. J., Mulvaney, R., Wolff, E. W., Triest, J., Kipfstuhl, S., Trusel, L. D., Vimeux, F., Fleet, L., and Arrowsmith, C.: Acceleration of snow melt in an Antarctic Peninsula ice core during the twentieth century, Nat. Geosci., 6, 404–411, https://doi.org/10.1038/ngeo1787, 2013.

Arrigo, K. R., Dijken, G. L., Castelao, R. M., Luo, H., Rennermalm, Å. K., Tedesco, M., Mote, T. L., Oliver, H., and Yager, P. L.: Melting glaciers stimulate large summer phytoplankton blooms in southwest Greenland waters, Geophys. Res. Lett., 44, 365   6278–6285, https://doi.org/10.1002/2017GL073583, 2017.

Ballantyne, C. K.: After the Ice: Holocene Geomorphic Activity in the Scottish Highlands, Scottish Geogr. J., 124, 8–52, https://doi.org/10.1080/14702540802300167, 2008.

Ban, Y., Gong, P., and Giri, C.: Global land cover mapping using Earth observation satellite data: Recent progresses and challenges, ISPRS J. Photogramm. Remote Sens., 103, 1–6, https://doi.org/10.1016/j.isprsjprs.2015.01.001, 2015.

370   Bannister, D. and King, J.: Föhn winds on South Georgia and their impact on regional climate, 70, 324–329, https://doi.org/10.1002/wea.2548, 2015.

Bañón, M., Justel, A., Velázquez, D., and Quesada, A.: Regional weather survey on Byers Peninsula, Livingston Island, South Shetland Islands, Antarctica, Antarct. Sci., 25, 146–156, https://doi.org/10.1017/S0954102012001046, 2013.

Banwell, A. F., Datta, R. T., Dell, R. L., Moussavi, M., Brucker, L., Picard, G., Shuman, C. A., and Stevens, L. A.: The 32-375   year record-high surface melt in 2019/2020 on the northern George VI Ice Shelf, Antarctic Peninsula, Cryosph., 15, 909–925, https://doi.org/10.5194/tc-15-909-2021, 2021.

Barták, M., Váczi, P., Stachoň, Z., and Kubešová, S.: Vegetation mapping of moss-dominated areas of northern part of James Ross Island (Antarctica) and a suggestion of protective measures, 5, 75–87, https://doi.org/10.5817/CPR2015-1-8, 2015.

Bentley, M. J., Hodgson, D. A., Smith, J. A., Cofaigh, C. Ó., Domack, E. W., Larter, R. D., Roberts, S. J., Brachfeld, S., Leventer, 380   A., Hjort, C., Hillenbrand, C.-D., and Evans, J.: Mechanisms of Holocene palaeoenvironmental change in the Antarctic Peninsula region, 19, 51–69, https://doi.org/10.1177/0959683608096603, 2009.

Bojinski, S., Verstraete, M., Peterson, T. C., Richter, C., Simmons, A., and Zemp, M.: The Concept of Essential Climate Variables in Support of Climate Research, Applications, and Policy, Bull. Am. Meteorol. Soc., 95, 1431–1443, https://doi.org/10.1175/BAMS-D-13-00047.1, 2014.

385   British Antarctic Survey: British Antarctic Territory geological map : scale 1:500,000 , Sheet 4, 1981.

Brown, C. F., Brumby, S. P., Guzder-Williams, B., Birch, T., Hyde, S. B., Mazzariello, J., Czerwinski, W., Pasquarella, V. J., Haertel, R., Ilyushchenko, S., Schwehr, K., Weisse, M., Stolle, F., Hanson, C., Guinan, O., Moore, R., and Tait, A. M.: Dynamic World, Near real-time global 10 m land use land cover mapping, Sci. Data, 9, 251, https://doi.org/10.1038/s41597-022-01307-4, 2022.

390   Brussaard, C. P. D., Wilhelm, S. W., Thingstad, F., Weinbauer, M. G., Bratbak, G., Heldal, M., Kimmance, S. A., Middelboe, M., Nagasaki, K., Paul, J. H., Schroeder, D. C., Suttle, C. A., Vaqué, D., and Wommack, K. E.: Global-scale processes with a

nanoscale drive: the role of marine viruses, ISME J., 2, 575–578, https://doi.org/10.1038/ismej.2008.31, 2008.

Burton-Johnson, A., Black, M., Fretwell, P. T., and Kaluza-Gilbert, J.: An automated methodology for differentiating rock from snow, clouds and sea in Antarctica from Landsat 8 imagery: a new rock outcrop map and area estimation for the entire

395   Antarctic continent, Cryosph., 10, 1665–1677, https://doi.org/10.5194/tc-10-1665-2016, 2016.

Cannone, N.: Geoecological responses, in: Past Antarctica, edited by: Oliva, M. and Ruiz-Fernández, J. B. T.-P. A., Elsevier, 201–216, https://doi.org/10.1016/B978-0-12-817925-3.00011-2, 2020.

Carrasco, J. F., Bozkurt, D., and Cordero, R. R.: A review of the observed air temperature in the Antarctic Peninsula. Did the warming trend come back after the early 21st hiatus?, Polar Sci., 28, 100653, https://doi.org/10.1016/j.polar.2021.100653,

400   2021.

Carrivick, J. L., Davies, B. J., Glasser, N. F., Nývlt, D., and Hambrey, M. J.: Late-Holocene changes in character and behaviour of land-terminating glaciers on James Ross Island, Antarctica, J. Glaciol., 58, 1176–1190, https://doi.org/10.3189/2012JoG11J148, 2012.

Chasmer, L., Mahoney, C., Millard, K., Nelson, K., Peters, D., Merchant, M., Hopkinson, C., Brisco, B., Niemann, O.,

405   Montgomery, J., Devito, K., and Cobbaert, D.: Remote Sensing of Boreal Wetlands 2: Methods for Evaluating Boreal Wetland Ecosystem State and Drivers of Change, Remote Sens., 12, 1321, https://doi.org/10.3390/rs12081321, 2020.

Chen, J., Chen, J., Liao, A., Cao, X., Chen, L., Chen, X., He, C., Han, G., Peng, S., Lu, M., Zhang, W., Tong, X., and Mills, J.: Global land cover mapping at 30m resolution: A POK-based operational approach, ISPRS J. Photogramm. Remote Sens., 103, 7–27, https://doi.org/10.1016/j.isprsjprs.2014.09.002, 2015.

410   Chen, W., Li, X., and Wang, L.: Fine Land Cover Classification in an Open Pit Mining Area Using Optimized Support Vector Machine and WorldView-3 Imagery, Remote Sens., 12, 82, https://doi.org/10.3390/rs12010082, 2019.

Chinn, T. and Mason, P.: The first 25 years of the hydrology of the Onyx River, Wright Valley, Dry Valleys, Antarctica, Polar Rec. (Gr. Brit)., 52, 16–65, https://doi.org/10.1017/S0032247415000212, 2016.

Cloern, J. E.: Turbidity as a control on phytoplankton biomass and productivity in estuaries, Cont. Shelf Res., 7, 1367–1381,

415   https://doi.org/10.1016/0278-4343(87)90042-2, 1987.

Collins, N. J.: The effects of volcanic activity on the vegetation of Deception Island, Br. Antarct. Surv. Bull., 21, 79–94, 1969.

Conovitz, P. A., Mcknight, D. M., Macdonald, L. H., Fountain, A. G., and House, H. R.: Hydrologic Processes Influencing Streamflow Variation in Fryxell Basin, Antarctica, na, 93–108, https://doi.org/10.1029/AR072p0093, 2013.

Costa, A., Molnar, P., Stutenbecker, L., Bakker, M., Silva, T. A., Schlunegger, F., Lane, S. N., Loizeau, J.-L., and Girardclos,

420   S.: Temperature signal in suspended sediment export from an Alpine catchment, Hydrol. Earth Syst. Sci., 22, 509–528, https://doi.org/10.5194/hess-22-509-2018, 2018.

Davies, B. J., Glasser, N. F., Carrivick, J. L., Hambrey, M. J., Smellie, J. L., and Nývlt, D.: Landscape evolution and ice-sheet behaviour in a semi-arid polar environment: James Ross Island, NE Antarctic Peninsula, Geol. Soc. London, Spec. Publ., 381, 353–395, https://doi.org/10.1144/SP381.1, 2013.

425   Davies, B. J., Hambrey, M. J., Glasser, N. F., Holt, T., Rodés, A., Smellie, J. L., Carrivick, J. L., and Blockley, S. P. E.: Ice-

dammed lateral lake and epishelf lake insights into Holocene dynamics of Marguerite Trough Ice Stream and George VI Ice Shelf, Alexander Island, Antarctic Peninsula, Quat. Sci. Rev., 177, 189–219, https://doi.org/10.1016/j.quascirev.2017.10.016, 2017.

Doran, P. T., Wharton, R. A., and Lyons, W. B.: Paleolimnology of the McMurdo Dry Valleys, Antarctica, J. Paleolimnol., 430   10, 85–114, https://doi.org/10.1007/BF00682507, 1994.

Doran, P. T., McKay, C. P., Clow, G. D., Dana, G. L., Fountain, A. G., Nylen, T., and Lyons, W. B.: Valley floor climate observations from the McMurdo dry valleys, Antarctica, 1986–2000, J. Geophys. Res. Atmos., 107, ACL 13-1-ACL 13-12, https://doi.org/10.1029/2001JD002045, 2002.

Engel, Z., Láska, K., Kavan, J., and Smolíková, J.: Persistent mass loss of Triangular Glacier, James Ross Island, north-eastern 435   Antarctic Peninsula, J. Glaciol., 1–13, https://doi.org/10.1017/jog.2022.42, 2022.

Farr, T. G., Rosen, P. A., Caro, E., Crippen, R., Duren, R., Hensley, S., Kobrick, M., Paller, M., Rodriguez, E., Roth, L., Seal, D., Shaffer, S., Shimada, J., Umland, J., Werner, M., Oskin, M., Burbank, D., and Alsdorf, D.: The Shuttle Radar Topography Mission, Rev. Geophys., 45, RG2004, https://doi.org/10.1029/2005RG000183, 2007.

Friedl, M. A., Sulla-Menashe, D., Tan, B., Schneider, A., Ramankutty, N., Sibley, A., and Huang, X.: MODIS Collection 5 440   global land cover: Algorithm refinements and characterization of new datasets, Remote Sens. Environ., 114, 168–182, https://doi.org/10.1016/j.rse.2009.08.016, 2010.

Friedlander, A. M., Goodell, W., Salinas-de-León, P., Ballesteros, E., Berkenpas, E., Capurro, A. P., Cárdenas, C. A., Hüne, M., Lagger, C., Landaeta, M. F., Muñoz, A., Santos, M., Turchik, A., Werner, R., and Sala, E.: Spatial patterns of continental shelf faunal community structure along the Western Antarctic Peninsula, PLoS One, 15, e0239895, 445   https://doi.org/10.1371/journal.pone.0239895, 2020.

Frohn, R. C., Reif, M., Lane, C., and Autrey, B.: Satellite remote sensing of isolated wetlands using object-oriented classification of Landsat-7 data, 29, 931–941, https://doi.org/10.1672/08-194.1, 2009.

Gao, L., Zhao, Y., Yang, Z., Liu, J., Liu, X., Zhang, S.-H., and Pei, J.: New Paleomagnetic and 40 Ar/ 39 Ar Geochronological Results for the South Shetland Islands, West Antarctica, and Their Tectonic Implications, J. Geophys. Res. Solid Earth, 123, 450   4–30, https://doi.org/10.1002/2017JB014677, 2018.

García-Rodríguez, F., Piccini, C., Carrizo, D., Sánchez-García, L., Pérez, L., Crisci, C., Oaquim, A. B. J., Evangelista, H., Soutullo, A., Azcune, G., and Lüning, S.: Centennial glacier retreat increases sedimentation and eutrophication in Subantarctic periglacial lakes: A study case of Lake Uruguay, Sci. Total Environ., 754, 142066, https://doi.org/10.1016/j.scitotenv.2020.142066, 2021.

455   GCOS: Implementation plan for the global observing system for climate in support of the UNFCCC (2010 update), https://library.wmo.int/doc_num.php?explnum_id=3851, 2010.

Gerrish, L., Fretwell, P., and Cooper, P.: High resolution vector polygons of Antarctic rock outcrop (7.3) [Data set], UK Polar Data Centre, Nat. Environ. Res. Counc. UK Res. Innov., https://doi.org/10.5285/cbacce42-2fdc-4f06-bdc2-73b6c66aa641, 2020.

460 Gong, P., Li, X., Wang, J., Bai, Y., Chen, B., Hu, T., Liu, X., Xu, B., Yang, J., Zhang, W., and Zhou, Y.: Annual maps of global artificial impervious area (GAIA) between 1985 and 2018, Remote Sens. Environ., 236, 111510, https://doi.org/10.1016/j.rse.2019.111510, 2020.

Gooseff, M. N., McKnight, D. M., Doran, P., Fountain, A. G., and Lyons, W. B.: Hydrological Connectivity of the Landscape of the McMurdo Dry Valleys, Antarctica, Geogr. Compass, 5, 666–681, https://doi.org/10.1111/j.1749-8198.2011.00445.x,
465 2011.

Guglielmin, M.: Past geomorphic processes: The role of permafrost and periglacial processes in ice-free environments, in: Past Antarctica, edited by: Oliva, M. and Ruiz-Fernández, J. B. T.-P. A., Elsevier, 125–137, https://doi.org/10.1016/B978-0-12-817925-3.00007-0, 2020.

Harangozo, S. A., Colwell, S. R., and King, J. C.: An analysis of a 34-year air temperature record from Fossil Bluff (71°S,
470 68°W), Antarctica, Antarct. Sci., 9, 355–363, https://doi.org/10.1017/S0954102097000436, 1997.

Heywood, R. B., Fuchs, V. E., and Laws, R. M.: A limnological survey of the Ablation Point area, Alexander Island, Antarctica, Philos. Trans. R. Soc. London. B, Biol. Sci., 279, 39–54, https://doi.org/10.1098/rstb.1977.0070, 1977.

Howat, I. M., Porter, C., Smith, B. E., Noh, M.-J., and Morin, P.: The Reference Elevation Model of Antarctica, Cryosph., 13, 665–674, https://doi.org/10.5194/tc-13-665-2019, 2019.

475 Hrbáček, F. and Uxa, T.: The evolution of a near-surface ground thermal regime and modeled active-layer thickness on James Ross Island, Eastern Antarctic Peninsula, in 2006–2016, Permafr. Periglac. Process., 31, 141–155, https://doi.org/10.1002/ppp.2018, 2020.

Humlum, O., Instanes, A., and Sollid, J. L.: Permafrost in Svalbard: a review of research history, climatic background and engineering challenges, Polar Res., 22, 191–215, https://doi.org/10.1111/j.1751-8369.2003.tb00107.x, 2003.

480 Jennings, S. J. A., Davies, B. J., Nývlt, D., Glasser, N. F., Engel, Z., Hrbáček, F., Carrivick, J. L., Mlčoch, B., and Hambrey, M. J.: Geomorphology of Ulu Peninsula, James Ross Island, Antarctica, J. Maps, 17, 125–139, https://doi.org/10.1080/17445647.2021.1893232, 2021.

Kavan, J.: Fluvial transport in the deglaciated Antarctic catchment – Bohemian Stream, James Ross Island, Geogr. Ann. Ser. A, Phys. Geogr., 1–10, https://doi.org/10.1080/04353676.2021.2010401, 2021.

485 Kavan, J., Ondruch, J., Nývlt, D., Hrbáček, F., Carrivick, J. L., and Láska, K.: Seasonal hydrological and suspended sediment transport dynamics in proglacial streams, James Ross Island, Antarctica, Geogr. Ann. Ser. A, Phys. Geogr., 99, 38–55, https://doi.org/10.1080/04353676.2016.1257914, 2017.

Kirkby, M. J. and Statham, I.: Surface Stone Movement and Scree Formation, J. Geol., 83, 349–362, https://doi.org/10.1086/628097, 1975.

490 Klaar, M. J., Kidd, C., Malone, E., Bartlett, R., Pinay, G., Chapin, F. S., and Milner, A.: Vegetation succession in deglaciated landscapes: implications for sediment and landscape stability, Earth Surf. Process. Landforms, 40, 1088–1100, https://doi.org/10.1002/esp.3691, 2015.

Kňažková, M., Nývlt, D., and Hrbáček, F.: Slope processes connected with snow patches in semi-arid ice-free areas of James

Ross Island, Antarctic Peninsula, 373, 107479, https://doi.org/10.1016/j.geomorph.2020.107479, 2021.

495 Laspoumaderes, C., Modenutti, B., Souza, M. S., Bastidas Navarro, M., Cuassolo, F., and Balseiro, E.: Glacier melting and stoichiometric implications for lake community structure: zooplankton species distributions across a natural light gradient, Glob. Chang. Biol., 19, 316–326, https://doi.org/10.1111/gcb.12040, 2013.

Leeuwe, M. A., Webb, A. L., Venables, H. J., Visser, R. J. W., Meredith, M. P., Elzenga, J. T. M., and Stefels, J.: Annual patterns in phytoplankton phenology in Antarctic coastal waters explained by environmental drivers, Limnol. Oceanogr., 65,
500 1651–1668, https://doi.org/10.1002/lno.11477, 2020.

Łepkowska, E. and Stachnik, Ł.: Which Drivers Control the Suspended Sediment Flux in a High Arctic Glacierized Basin (Werenskioldbreen, Spitsbergen)?, 10, 1408, https://doi.org/10.3390/w10101408, 2018.

Loveland, T. R., Reed, B. C., Brown, J. F., Ohlen, D. O., Zhu, Z., Yang, L., and Merchant, J. W.: Development of a global land cover characteristics database and IGBP DISCover from 1 km AVHRR data, Int. J. Remote Sens., 21, 1303–1330,
505 https://doi.org/10.1080/014311600210191, 2000.

Maat, D. S., Visser, R. J. W., and Brussaard, C. P. D.: Virus removal by glacier-derived suspended fine sediment in the Arctic, J. Exp. Mar. Bio. Ecol., 521, 151227, https://doi.org/10.1016/j.jembe.2019.151227, 2019.

Malinowski, R., Lewiński, S., Rybicki, M., Gromny, E., Jenerowicz, M., Krupiński, M., Nowakowski, A., Wojtkowski, C., Krupiński, M., Krätzschmar, E., and Schauer, P.: Automated Production of a Land Cover/Use Map of Europe Based on
510 Sentinel-2 Imagery, Remote Sens., 12, 3523, https://doi.org/10.3390/rs12213523, 2020.

Marchant, D. R. and Head, J. W.: Antarctic dry valleys: Microclimate zonation, variable geomorphic processes, and implications for assessing climate change on Mars, Icarus, 192, 187–222, https://doi.org/10.1016/j.icarus.2007.06.018, 2007.

Martin, P. J. and Peel, D. A.: The Spatial Distribution of 10 m Temperatures in the Antarctic Peninsula, J. Glaciol., 20, 311–317, https://doi.org/10.3189/S0022143000013861, 1978.

515 Mink, S., López-Martínez, J., Maestro, A., Garrote, J., Ortega, J. A., Serrano, E., Durán, J. J., and Schmid, T.: Insights into deglaciation of the largest ice-free area in the South Shetland Islands (Antarctica) from quantitative analysis of the drainage system, 225, 4–24, https://doi.org/10.1016/j.geomorph.2014.03.028, 2014.

Mlčoch, B., Nývlt, D., and Mixa, P.: Geological map of James Ross Island–Northern part 1: 25,000, 2020.

Mulvaney, R., Abram, N. J., Hindmarsh, R. C. A., Arrowsmith, C., Fleet, L., Triest, J., Sime, L. C., Alemany, O., and Foord,
520 S.: Recent Antarctic Peninsula warming relative to Holocene climate and ice-shelf history, Nature, 489, 141–144, https://doi.org/10.1038/nature11391, 2012.

Nedbalová, L., Nývlt, D., Kopáček, J., Šobr, M., and Elster, J.: Freshwater lakes of Ulu Peninsula, James Ross Island, north-east Antarctic Peninsula: origin, geomorphology and physical and chemical limnology, Antarct. Sci., 25, 358–372, https://doi.org/10.1017/S0954102012000934, 2013.

525 Nývlt, D., Fišáková, M. N., Barták, M., Stachoň, Z., Pavel, V., Mlčoch, B., and Láska, K.: Death age, seasonality, taphonomy and colonization of seal carcasses from Ulu Peninsula, James Ross Island, Antarctic Peninsula, Antarct. Sci., 28, 3–16, https://doi.org/10.1017/S095410201500036X, 2016.

Oliva, M., Antoniades, D., Giralt, S., Granados, I., Pla-Rabes, S., Toro, M., Liu, E. J., Sanjurjo, J., and Vieira, G.: The Holocene deglaciation of the Byers Peninsula (Livingston Island, Antarctica) based on the dating of lake sedimentary records, 261, 89–
530 102, https://doi.org/10.1016/j.geomorph.2016.02.029, 2016.

Oliva, M., Navarro, F., Hrbáček, F., Hernández, A., Nývlt, D., Pereira, P., Ruiz-Fernández, J., and Trigo, R.: Recent regional climate cooling on the Antarctic Peninsula and associated impacts on the cryosphere, Sci. Total Environ., 580, 210–223, https://doi.org/10.1016/j.scitotenv.2016.12.030, 2017.

Olofsson, P., Foody, G. M., Stehman, S. V, and Woodcock, C. E.: Making better use of accuracy data in land change studies:
535 Estimating accuracy and area and quantifying uncertainty using stratified estimation, Remote Sens. Environ., 129, 122–131, https://doi.org/10.1016/j.rse.2012.10.031, 2013.

Olofsson, P., Foody, G. M., Herold, M., Stehman, S. V, Woodcock, C. E., and Wulder, M. A.: Good practices for estimating area and assessing accuracy of land change, Remote Sens. Environ., 148, 42–57, https://doi.org/10.1016/j.rse.2014.02.015, 2014.

540 Overeem, I., Hudson, B. D., Syvitski, J. P. M., Mikkelsen, A. B., Hasholt, B., van den Broeke, M. R., Noël, B. P. Y., and Morlighem, M.: Substantial export of suspended sediment to the global oceans from glacial erosion in Greenland, Nat. Geosci., 10, 859–863, https://doi.org/10.1038/ngeo3046, 2017.

Pannewitz, S., Green, T. G. A., Scheidegger, C., Schlensog, M., and Schroeter, B.: Activity pattern of the moss Hennediella heimii (Hedw.) Zand. in the Dry Valleys, Southern Victoria Land, Antarctica during the mid-austral summer, Polar Biol., 26,
545 545–551, https://doi.org/10.1007/s00300-003-0518-8, 2003.

Pazúr, R., Huber, N., Weber, D., Ginzler, C., and Price, B.: A national extent map of cropland and grassland for Switzerland based on Sentinel-2 data, Earth Syst. Sci. Data, 14, 295–305, https://doi.org/10.5194/essd-14-295-2022, 2022.

Petford, N. and Mirhadizadeh, S.: Image-based modelling of lateral magma flow: the Basement Sill, Antarctica, R. Soc. Open Sci., 4, 161083, https://doi.org/10.1098/rsos.161083, 2017.

550 Raup, B., Racoviteanu, A., Khalsa, S. J. S., Helm, C., Armstrong, R., and Arnaud, Y.: The GLIMS geospatial glacier database: A new tool for studying glacier change, Glob. Planet. Change, 56, 101–110, https://doi.org/https://doi.org/10.1016/j.gloplacha.2006.07.018, 2007.

Righetti, D., Vogt, M., Gruber, N., Psomas, A., and Zimmermann, N. E.: Global pattern of phytoplankton diversity driven by temperature and environmental variability, Sci. Adv., 5, eaau6253, https://doi.org/10.1126/sciadv.aau6253, 2019.

555 Roman, M., Nedbalová, L., Kohler, T. J., Lirio, J. M., Coria, S. H., Kopáček, J., Vignoni, P. A., Kopalová, K., Lecomte, K. L., Elster, J., and Nývlt, D.: Lacustrine systems of Clearwater Mesa (James Ross Island, north-eastern Antarctic Peninsula): geomorphological setting and limnological characterization, Antarct. Sci., 31, 169–188, https://doi.org/10.1017/S0954102019000178, 2019.

Rosa, K. K. da, Perondi, C., Veettil, B. K., Auger, J. D., and Simões, J. C.: Contrasting responses of land-terminating glaciers
560 to recent climate variations in King George Island, Antarctica, Antarct. Sci., 32, 398–407, https://doi.org/10.1017/S0954102020000279, 2020.

Rosado, B., Fernández-Ros, A., Berrocoso, M., Prates, G., Gárate, J., de Gil, A., and Geyer, A.: Volcano-tectonic dynamics of Deception Island (Antarctica): 27 years of GPS observations (1991–2018), J. Volcanol. Geotherm. Res., 381, 57–82, https://doi.org/10.1016/j.jvolgeores.2019.05.009, 2019.

565 Salvatore, M. C.: Geomorphological sketch map of the Fossil Bluff area (Alexander Island, Antarctica) mapped from aerial photographs, Antarct. Sci., 13, 75–78, https://doi.org/10.1017/S0954102001000116, 2001.

Secretariat of the Antarctic Treaty: ASPA 140: Parts of Deception Island, South Shetland Islands, 2022.

Smellie, J. L. and Martin, A. P.: Chapter 5.2a Erebus Volcanic Province: volcanology, Geol. Soc. London, Mem., 55, 415–446, https://doi.org/10.1144/M55-2018-62, 2021.

570 Smellie, J. L., López-Martínez, J., Headland, R. K., Hernández-Cifuentes, F., Maestro, A., Millar, I. L., Rey, J., Serrano, E., Somoza, L., and Thomson, J. W.: Geology and geomorphology of Deception Island, British Antarctic Survey, 2002.

Smith, R. I. L.: Botanical survey of Deception Island, Br. Antarct. Surv. Bull., 129–136, 1988.

Smith, R. I. L.: The thermophilic bryoflora of Deception Island: Unique plant communities as a criterion for designating an Antarctic Specially Protected Area, Antarct. Sci., 17, 17–27, https://doi.org/10.1017/S0954102005002385, 2005.

575 Sommaruga, R.: When glaciers and ice sheets melt: consequences for planktonic organisms, J. Plankton Res., 37, 509–518, https://doi.org/10.1093/plankt/fbv027, 2015.

Staines, K. E. H., Carrivick, J. L., Tweed, F. S., Evans, A. J., Russell, A. J., Jóhannesson, T., and Roberts, M.: A multi-dimensional analysis of pro-glacial landscape change at Sólheimajökull, southern Iceland, Earth Surf. Process. Landforms, 40, 809–822, https://doi.org/10.1002/esp.3662, 2015.

580 Stringer, C. D.: Contemporary (2016–2020) land cover across West Antarctica and the McMurdo Dry Valleys [Code] (Version 1). Zenodo. https://doi.org/10.5281/zenodo.6720051 , 2022

Stringer, C.: Contemporary (2016 - 2020) land cover classification across West Antarctica and the McMurdo Dry Valleys (Version 1.0) [Data set]. NERC EDS UK Polar Data Centre. https://doi.org/10.5285/5A5EE38C-E296-48A2-85D2-E29DB66E5E24, 2022

585 Strother, S. L., Salzmann, U., Roberts, S. J., Hodgson, D. A., Woodward, J., Van Nieuwenhuyze, W., Verleyen, E., Vyverman, W., and Moreton, S. G.: Changes in Holocene climate and the intensity of Southern Hemisphere Westerly Winds based on a high-resolution palynological record from sub-Antarctic South Georgia, 25, 263–279, https://doi.org/10.1177/0959683614557576, 2015.

Syvitski, J. P. M.: Sediment discharge variability in Arctic rivers: implications for a warmer future, Polar Res., 21, 323–330,
590 https://doi.org/10.3402/polar.v21i2.6494, 2002.

Tateishi, R., Hoan, N. T., Kobayashi, T., Alsaaideh, B., Tana, G., and Phong, D. X.: Production of Global Land Cover Data – GLCNMO2008, J. Geogr. Geol., 6, 99–123, https://doi.org/10.5539/jgg.v6n3p99, 2014.

Tejedo, P., Benayas, J., Cajiao, D., Albertos, B., Lara, F., Pertierra, L. R., Andrés-Abellán, M., Wic, C., Luciáñez, M. J., Enríquez, N., Justel, A., and Reck, G. K.: Assessing environmental conditions of Antarctic footpaths to support management
595 decisions, J. Environ. Manage., 177, 320–330, https://doi.org/10.1016/j.jenvman.2016.04.032, 2016.

Tejedo, P., Benayas, J., Cajiao, D., Leung, Y.-F., De Filippo, D., and Liggett, D.: What are the real environmental impacts of Antarctic tourism? Unveiling their importance through a comprehensive meta-analysis, J. Environ. Manage., 308, 114634, https://doi.org/10.1016/j.jenvman.2022.114634, 2022.

Vaughan, D. G., Marshall, G. J., Connolley, W. M., Parkinson, C., Mulvaney, R., Hodgson, D. A., King, J. C., Pudsey, C. J.,
600 and Turner, J.: Recent Rapid Regional Climate Warming on the Antarctic Peninsula, Clim. Change, 60, 243–274, https://doi.org/10.1023/A:1026021217991, 2003.

Walker, D. A., Daniëls, F. J. A., Matveyeva, N. V, Šibík, J., Walker, M. D., Breen, A. L., Druckenmiller, L. A., Raynolds, M. K., Bültmann, H., Hennekens, S., Buchhorn, M., Epstein, H. E., Ermokhina, K., Fosaa, A. M., Hei∂marsson, S., Heim, B., Jónsdóttir, I. S., Koroleva, N., Lévesque, E., MacKenzie, W. H., Henry, G. H. R., Nilsen, L., Peet, R., Razzhivin, V., Talbot,
605 S. S., Telyatnikov, M., Thannheiser, D., Webber, P. J., and Wirth, L. M.: Circumpolar Arctic Vegetation Classification, 48, 181–201, https://doi.org/10.1127/phyto/2017/0192, 2018.

Appendices

Appendix A: Accuracy matrices

A1: Accuracy matrix for all land cover types

Class	Reference classes						Total (ni)	Total area (km2)	Wi	Wi2
	Water (1)	Ice (4)	Bedrock (6)	Coarse Sed (7)	Fine Sed (8)	Veg (9)				
Water	5	3	0	0	0	1	9	9E+01	2E-03	4E-06
Ice	1	2588	0	4	2	0	2595	4E+04	9E-01	8E-01
Bedrock	0	4	11	4	7	1	27	2E+02	5E-03	2E-05
Coarse Sed	0	48	0	55	11	0	114	1E+03	3E-02	9E-04
Fine Sed	0	20	3	4	107	0	134	2E+03	5E-02	3E-03
Veg	0	0	0	3	2	5	10	2E+02	3E-03	1E-05
Total (nj)	6	2663	14	70	129	7	2889	47735.7975		
No data	0	65	1	22	22	3				

Class	Water	Ice	Bedrock	Coarse	Fine	Veg	Total (p̂i)	Ûi	p̂j
Water	0.00	0.00	0.00	0.00	0.00	0.00	0.00	0.56	0.83
Turbid	0.00	0.90	0.00	0.00	0.00	0.00	0.90	1.00	0.97
Bedrock	0.00	0.00	0.00	0.00	0.00	0.00	0.01	0.41	0.79
Fine Sed	0.00	0.02	0.00	0.02	0.00	0.00	0.04	0.48	0.79
Coarse Sed	0.00	0.01	0.00	0.00	0.04	0.00	0.05	0.80	0.83
Veg	0.00	0.00	0.00	0.00	0.00	0.00	0.00	0.50	0.71
Total (p̂j)	0.00	0.92	0.00	0.02	0.04	0.00	1.00	3.74	4.92

Class	Error adjusted area	95% confidence	% Area	% error	n		Overall accuracy	95.92%
Water	99	46	0.21%	45.92%	9			
Ice	44,002	220	92.18%	0.50%	2,595			
Bedrock	231	174	0.48%	75.32%	27			
Fine Sed	2,132	196	4.47%	9.19%	134			
Coarse Sed	1,157	174	2.42%	15.06%	114			
Veg	116	56	0.24%	48.76%	10			
610 Total	47,735.80							

A2: Accuracy matrix of proglacial classes

Class	Reference classes						Total (ni)	Total area (km2)	Wi	Wi2
	Water (1)	Ice (4)	Bedrock (6)	Coarse Sed (7)	Fine Sed (8)	Veg (9)				
Water	11	0	0	1	2	1	15	9.17E+01	0.02	0.00
Ice	2	0	3	16	16	1	38	0.00E+00	0.00	0.00
Bedrock	0	0	30	12	3	0	45	2.36E+02	0.05	0.00
Coarse Sed	2	0	14	190	51	0	257	1.46E+03	0.34	0.11
Fine Sed	0	0	3	28	335	5	371	2.40E+03	0.55	0.31
Veg	0	0	0	6	9	19	34	1.53E+02	0.04	0.00
Total (nj)	15	0	50	253	416	26	760	4339.899		
No data	7		5	84	197	10				

Class	Water	Ice	Bedrock	Coarse	Fine	Veg	Total (p̂i)	Ûi	p̂j
Water	0.01	0.00	0.00	0.00	0.00	0.00	0.02	0.73	0.73
Ice	0.00	0.00	0.00	0.02	0.02	0.00	0.05	0.00	0.00
Bedrock	0.00	0.00	0.04	0.02	0.00	0.00	0.06	0.67	0.60
Fine Sed	0.00	0.00	0.02	0.25	0.07	0.00	0.34	0.74	0.75
Coarse Sed	0.00	0.00	0.00	0.04	0.44	0.01	0.49	0.90	0.81
Veg	0.00	0.00	0.00	0.01	0.01	0.03	0.04	0.56	0.73
Total (p̂j)	0.02	0.00	0.07	0.33	0.55	0.03	1.00	3.60	3.62

Class	Error adjusted area	95% confidence	% Area	% error	n		Overall accuracy	76.97%
Water	86	26	1.97%	30.87%	15			
Bedrock	286	57	6.58%	19.86%	45			
Fine Sed	2,376	107	54.74%	4.50%	371			
Coarse Sed	1,445	109	33.29%	7.53%	257			
Veg	148	40	3.42%	26.99%	34			
Total	4,340							

615

620

625

Appendix B: Images used in analysis

B1: Images used during the analysis, including the date of image acquisition and overall cloud cover

Image ID	Date	Overall % cloud cover
James Ross Island		
LANDSAT/LC08/C01/T2_TOA/LC08_215105_20170204	04/02/2017	12.66
LANDSAT/LC08/C01/T2_TOA/LC08_215105_20160202	02/02/2016	5.8
Dry Valleys		
LANDSAT/LC08/C01/T2_TOA/LC08_056116_20191115	15/11/2019	0.08
LANDSAT/LC08/C01/T2_TOA/LC08_061115_20191118	18/11/2019	0.14
LANDSAT/LC08/C01/T2_TOA/LC08_061114_20191102	02/11/2019	0.07
Alexander Island		
LANDSAT/LC08/C01/T2_TOA/LC08_217110_20191209	09/12/2019	0.47
LANDSAT/LC08/C01/T2_TOA/LC08_217111_20191107	07/11/2019	0.64
LANDSAT/LC08/C01/T2_TOA/LC08_216110_20191218	18/12/2019	0.22
Deception Island		
LANDSAT/LC08/C01/T2_TOA/LC08_219104_20200209	09/02/2020	20.74
Byers Peninsula		
LANDSAT/LC08/C01/T2_TOA/LC08_219104_20200209	09/02/2020	20.74
South Georgia		
LANDSAT/LC08/C01/T1_TOA/LC08_205098_20180116	28/03/2018	2.45
LANDSAT/LC08/C01/T1_TOA/LC08_207098_20180404	04/04/2018	46.98

Figures
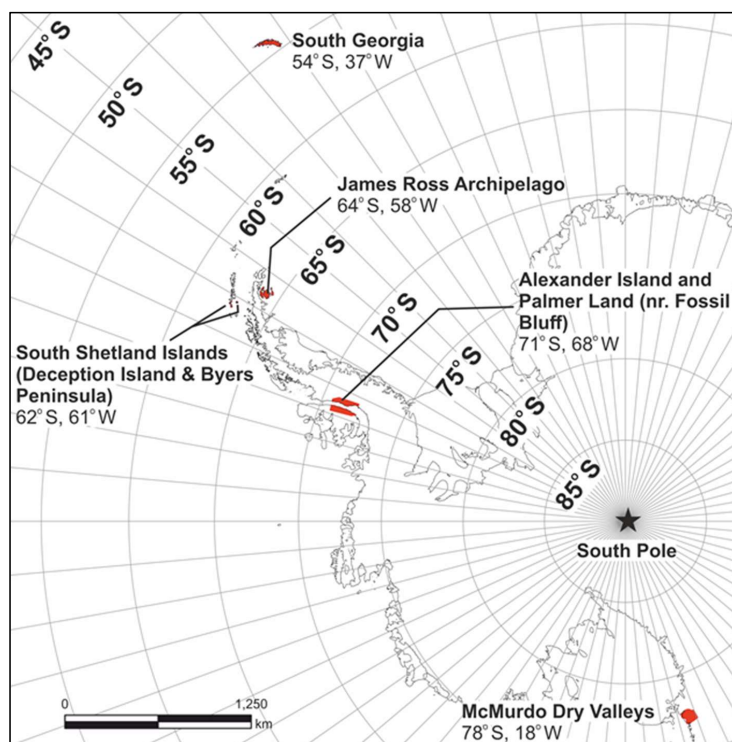
Figure 1: A map of our study sites. The areas analysed have been highlighted in red, with their latitude and longitude displayed to highlight the latitudinal gradient of the selected sites

630
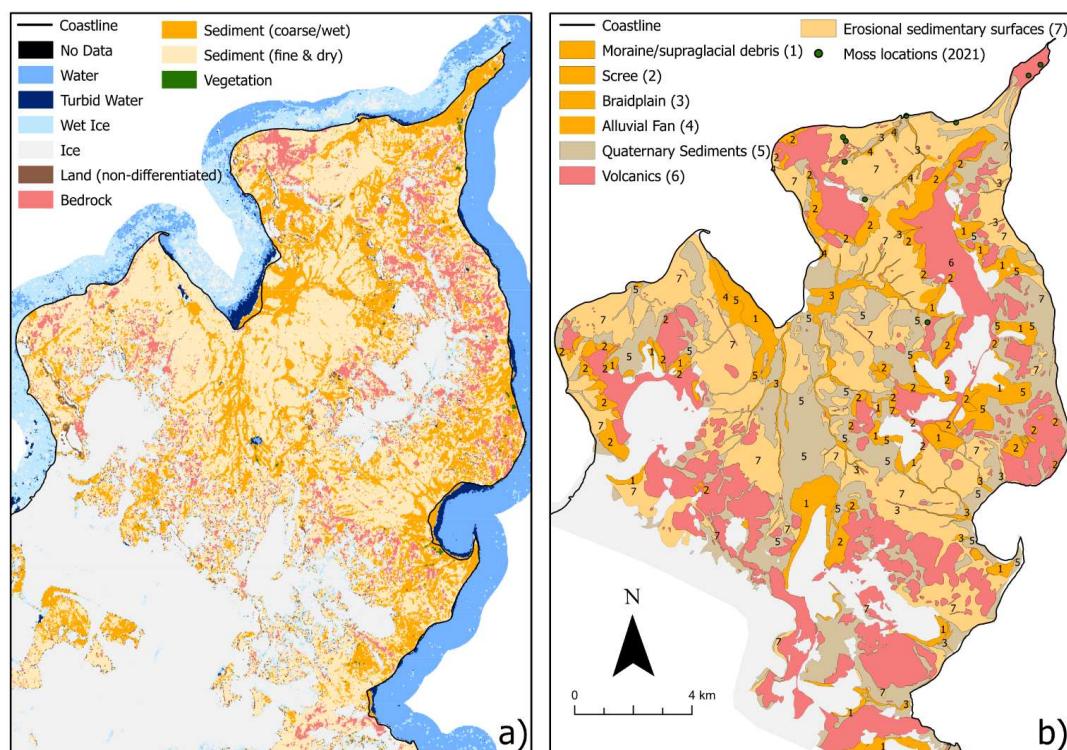
Figure 2: Two classifications of the Ulu Peninsula on James Ross Island, a) A classification of the Ulu Peninsula, produced in this study; b) a map adapted from Jennings et al. (2021), displaying data collected through remote sensing and fieldwork. Vegetation locations as collected by Jan Kavan (of CARP) in 2021 are also displayed. Note the similarities in the ice class, locations of river systems, and scree slopes. NB: the colours in panel b have been adapted to allow a more direct comparison with the map produced in this study (a).
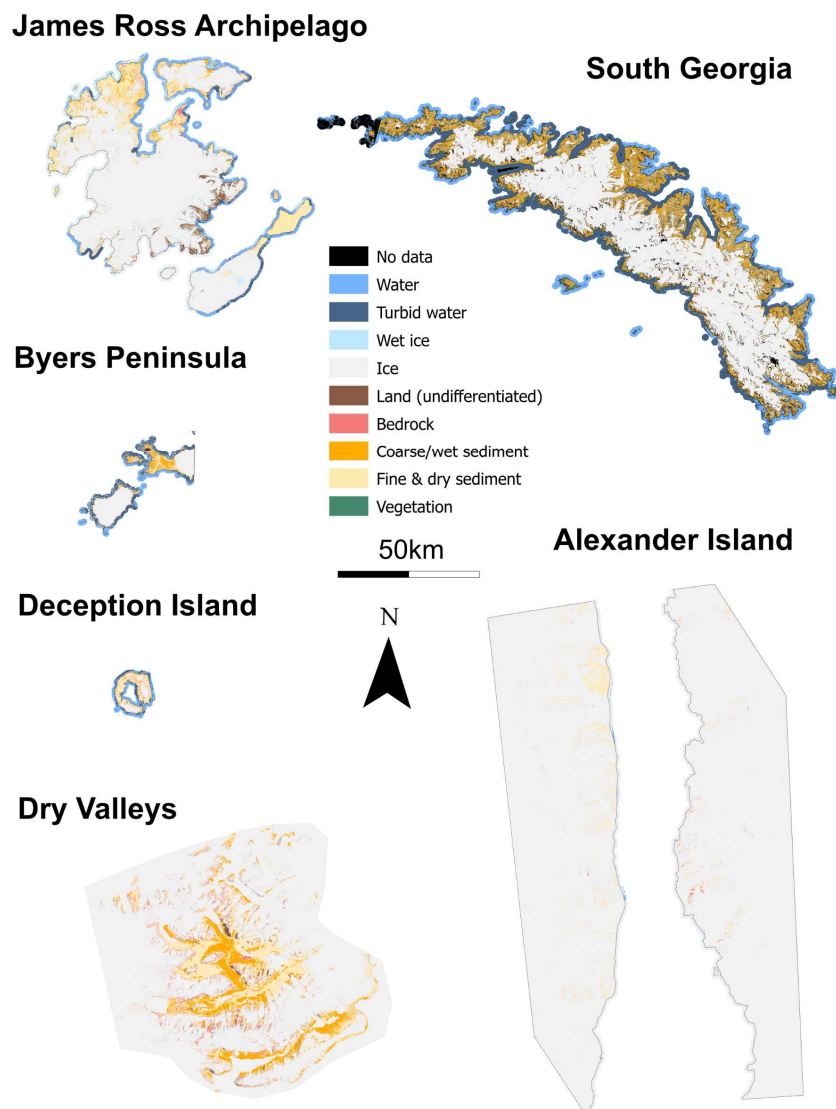
Figure 3: Land cover maps of the six sites, including 10 classes, which describe eight distinct surfaces
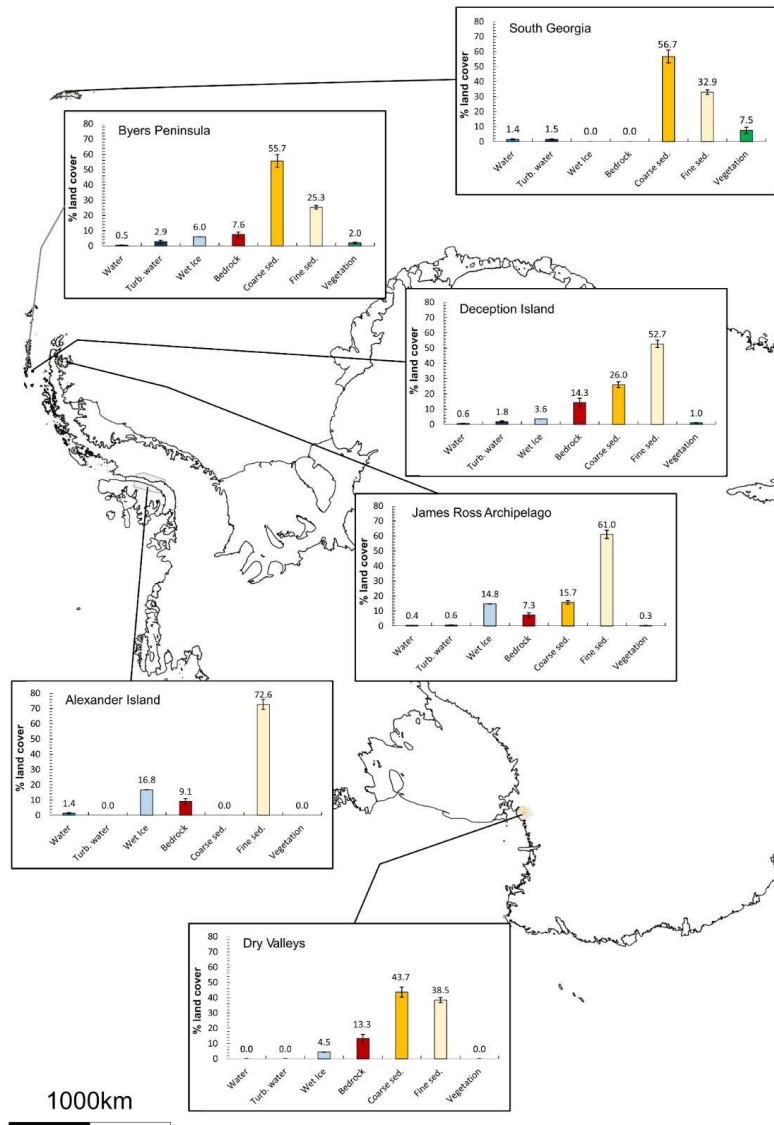
Figure 4: Percentage land cover values (excluding ice, no data and land (undifferentiated)) for each site, overlaying the coastline of Antarctica (coastline sourced from BAS). Error bars indicate the 95% confidence intervals.
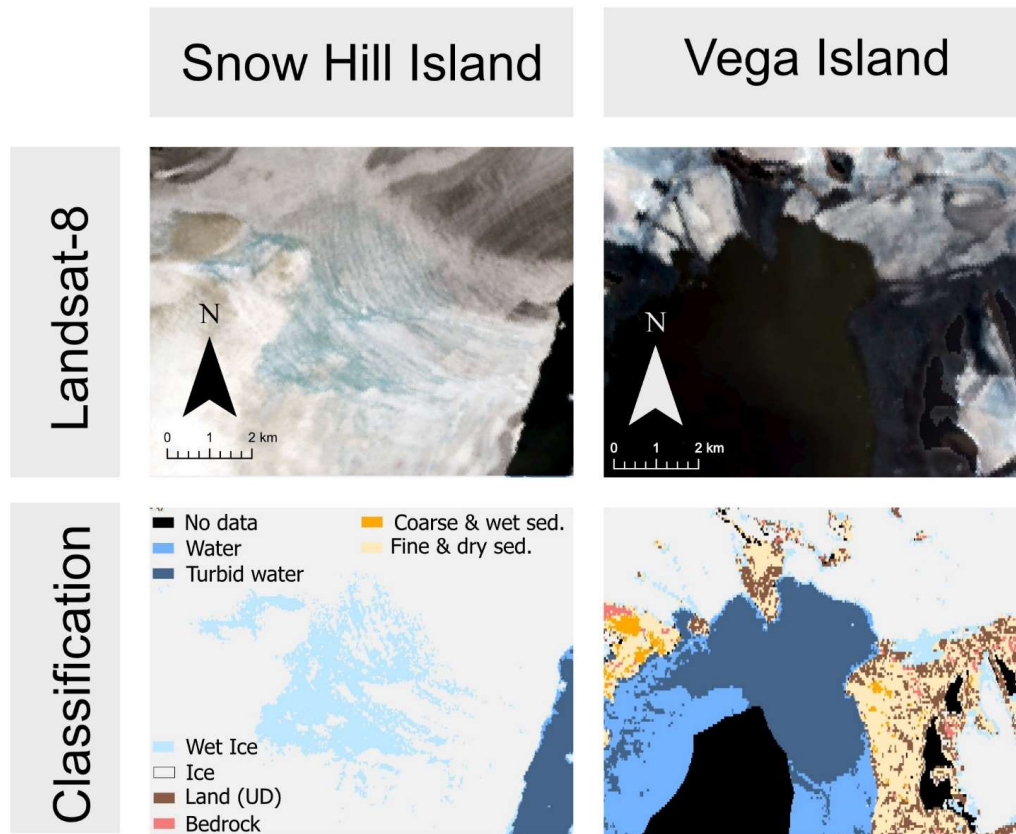
Figure 5: How the wet ice and turbid water classes compare to the images they are derived from, with a large area of saturated firn on Snow Hill Island, and a sediment plume off the coast of Vega Island

670

675
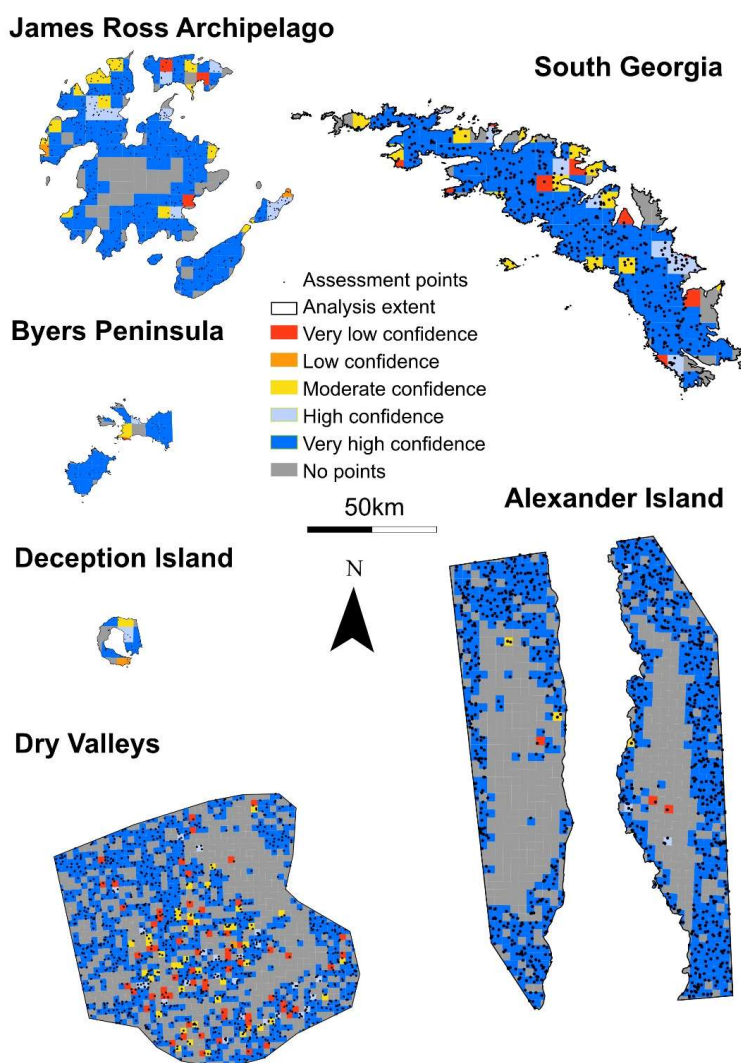
Figure 6: Maps of each site indicating the spatial variability in confidence. Very low confidence = <20% of points were accurate; low confidence = 21 to 40%; medium confidence = 41 to 60%; high confidence = 61% to 80%; very high confidence = >80%